Randomly Forced Wave Equation in Photonic Crystals

Chia Ying Lee

August 9, 2007

1 Introduction

A photonic crystal is an optical material comprised of materials of different refractive indices interspersed and arranged in a lattice structure. The arrangement of these materials within the photonic crystal is periodic, and the shortest period is called the lattice constant. Due to the interspersion of materials of different refractive indices and electrical permittivities, electromagnetic waves passing through the photonic crystal will be scattered in a very specific way. This results in many interesting and useful optical properties being exhibited by photonic crystals, which causes it to be the topic of active research at present.

Photonic crystals can be classified as 1,2 or 3-dimensional. We will be considering only the 2-dimensional photonic crystal in this paper, which we hereby describe. Along the $x-y$ planar cross-section, one material of permittivity ϵ_a occurs in disks of radius r_a, centered on lattice grid points that are the lattice constant a apart. A second material with permittivity ϵ_b occupies the remaining space. The two materials extend uniformly along the z-axis.

In this paper, we study a method of simulating the propagation of an electric field through a photonic crystal, induced by a random current source.

1.1 The Wave Equation

For the purposes of this paper, we adopt the model setup of the 2-D photonic crystals used in [1]. The main equation in consideration is the 2-dimensional wave equation

$$\triangle E_z(x,y,t) - \mu\epsilon(x,y)\frac{\partial^2 E_z}{\partial t^2}(x,y,t) = \mu\frac{\partial J_z}{\partial t}(x,y,t) \tag{1.1}$$

describing the propagation in the xy plane of the z-component of the electric field $\mathbf{E} = (E_x, E_y, E_z)$ when driven by a current source $\mathbf{J} = (J_x, J_y, J_z)$. μ and ϵ are the permeability and permittivity of the medium, respectively. We assume μ to be the permeability of free space, since we assume that the photonic crystals are not magnetic materials [4]. Due to the regularity of the PC lattice structure, we also assume that $\epsilon(x,y)$ is periodic in both the x- and y-directions, with

period equal to the lattice constant. The 2-dimensional setting also allows us to assume that all space dependent variables are independent of z. In particular,

$$\frac{\partial E_z}{\partial z} = \frac{\partial H_z}{\partial z} = 0 \tag{1.2}$$

Eq. (1.1) is a special case of the more general wave equation derived from the Maxwell equations (see for e.g. [3]).

$$\begin{aligned} \nabla \cdot \mathbf{D}(\mathbf{x}, t) &= \rho & (1.3)\\ \nabla \cdot \mathbf{B}(\mathbf{x}, t) &= 0 & (1.4)\\ \nabla \times \mathbf{E}(\mathbf{x}, t) &= -\frac{\partial}{\partial t}\mathbf{B}(\mathbf{x}, t) & (1.5)\\ \nabla \times \mathbf{H}(\mathbf{x}, t) &= \mathbf{J} + \frac{\partial}{\partial t}\mathbf{D}(\mathbf{x}, t) & (1.6) \end{aligned}$$

where $\mathbf{x} = (x, y, z)$ is the 3-dimensional spatial vector. The other symbols: $\mathbf{E}$ and $\mathbf{D}$ are the electric field and flux, respectively; $\mathbf{H}$ and $\mathbf{B}$ are the magnetic field and flux, respectively; and, ρ and $\mathbf{J}$ are the charge and current densities, respectively. The constitutive relations tell us that $\mathbf{D} = \epsilon\mathbf{E}$ and $\mathbf{B} = \mu\mathbf{H}$, and together with (1.2) lead to the wave equation Eq. (1.1). A similar wave equation holds for H_z, but we shall not consider this equation here.

1.2 A Physical Model for Simulation

The model set up in [1] consists of a $[0, X] \times [0, Y]$ PC lattice structure with a current source placed along one edge, $x = 0$, of the PC structure. The source provides a current density $\mathbf{J}$ that is spatially incoherent in the y direction. The intensities of the induced electric field is then measured along the opposite edge at $x = X$. The incoherence of the current source is modelled using a spatial white noise $\dot{W}(y)$ on $[0, Y]$

$$J(x, y, t) = \mathbf{1}_{(x=0)} V_A(t) \dot{W}(y) \tag{1.7}$$

with

$$V_A(t) = \sin(\omega t) e^{-(\frac{t}{T_0})^2} \tag{1.8}$$

For convenience, we have dropped the z subscripts to write J in place of J_z, since all the action happens in the z component. Similarly we write E in place of E_z.

We shall be more specific with the form of the spatial white noise we use. Let $V_y = L_2([0, Y])$ and $\{m_i(y)\}_{y=0}^{\infty}$ be the following orthonormal basis of V_y

$$\begin{aligned} m_0(y) &= \frac{1}{\sqrt{Y}} \\ m_i(y) &= \sqrt{\frac{2}{Y}} \cos(\frac{(i-1)\pi y}{Y}), \quad i = 2, 3, \ldots & (1.9) \end{aligned}$$

Let $W(y)$ be a Brownian motion on $[0, Y]$. We let $\mathrm{L}_2(\mathbb{F})$ denote the space of square integrable random variables. For $i = 1, 2, \dots$ we define the independent Gaussian random variables

$$\xi_i = \int_0^Y m_i(y) dW(y) \tag{1.10}$$

from which we obtain the expression for the white noise

$$\dot{W}(y) = \sum_{i=1}^{\infty} \xi_i m_i(y) \tag{1.11}$$

The collection of multi-indices $\mathcal{J}$ consist of elements of the form $\alpha = (\alpha_1, \alpha_2, \dots)$. It is well-known that an orthonormal basis in $L_2(\mathbb{F})$ is the Hermite polynomial basis $\{\xi_\alpha\}_{\alpha \in \mathcal{J}}$, where

$$\xi_\alpha = \prod_{k=1}^{\infty} \frac{H_{\alpha_k}(\xi_k)}{\sqrt{\alpha_k}} \tag{1.12}$$

In view of Eq. (1.11) and (1.12), we see that the Fourier coefficients J_α of J (with respect to ξ_α) are non-zero only when $|\alpha| = 1$. Denoting J_i to be the Fourier coefficient of such α with $\alpha_i = 1$, we obtain the Fourier expansion

$$J(x, y, t) = \sum_{i=1}^{\infty} J_i(x, y, t)\xi_i = \sum_{i=1}^{\infty} \mathbf{1}_{(x=0)} V_A(t) m_i(y) \xi_i \tag{1.13}$$

2 Solving the Wave Equation

2.1 The Skeleton Equations of the Wave Equation

The randomness incorporated by the incoherent source J turns Eq. (1.1) into an SPDE. By knowing the Fourier coefficients E_α of E, we will be able to gleam information on the solution's moments, as well as simulate approximations to individual realizations of the solution.

Taking Eq. (1.1), we multiply both sides by ξ_α, and take the expectation to obtain an identical PDE for the Fourier coefficients

$$\triangle E_\alpha(x, y, t) - \mu\epsilon(x, y) \frac{\partial^2 E_\alpha}{\partial t^2}(x, y, t) = \mu \frac{\partial J_\alpha}{\partial t}(x, y, t) \tag{2.1}$$

System (2.1) is known as the *skeleton equations* or *propagator* of the wave equation. The crucial difference now is that each equation in (2.1) is a *deterministic* PDE, and can be solved numerically using known methods.

It may seem like an intractable number of coefficients to compute, but fortunately, for our special choice of current source (1.13), the number of non-trivial coefficients can be significantly reduced. For, observe that if $|\alpha| \neq 1$, $J_\alpha \equiv 0$

implies that (2.1) has the trivial solution $E_\alpha \equiv 0$ (with zero boundary conditions). Hence, the skeleton equations reduce to the following system of PDEs for $i = 1, 2, \ldots$

$$\triangle E_i(x,y,t) - \mu\epsilon(x,y)\frac{\partial^2 E_i}{\partial t^2}(x,y,t) = \mu \mathbf{1}_{(x=0)} V_A'(t) m_i(y) \tag{2.2}$$

where E_i is the coefficient of ξ_i. The exact solution of E can be found by

$$E(x,y,t) = \sum_{i=1}^{\infty} E_i(x,y,t)\xi_i \tag{2.3}$$

Remark The above spectral analysis is a more general approach than the approach proposed in [1]. The authors propose first Fourier expanding the solution with respect to the basis $\{m_i(y)\}$ in V_y, after which the high frequency modes (large i) are truncated. We shall see that for our special choice of $\mathbf{J}$, namely for the stochasticity in $\mathbf{J}$ to involve only white noise, the two approaches coincide.

For simplicity, let us assume ϵ to be a constant. Taking the inner product with $m_i(y)$, $i = 1, 2, \ldots$ on both sides of Eq. (1.1) yields an SPDE for the Fourier coefficients u_i of E

$$\frac{\partial^2 u_i}{\partial x^2}(x,t) + \kappa_i u_i(x,t) - \mu\epsilon\frac{\partial^2 u_i}{\partial t^2}(x,t) = \mu\frac{\partial v_i}{\partial t}(x,t) \tag{2.4}$$

where $v_i(x,t) = \mathbf{1}_{x=0} V(t)\xi_i$ are the Fourier coefficients of J, and κ_i satisfies $m_i''(y) = \kappa_i m_i(y)$. Then the coefficients of u_i with respect to ξ_α are

$$\frac{\partial^2 u_{i,\alpha}}{\partial x^2}(x,t) + \kappa_i u_{i,\alpha}(x,t) - \mu\epsilon\frac{\partial^2 u_{i,\alpha}}{\partial t^2}(x,t) = \mu \mathbf{1}_{x=0} V_A'(t)\delta_{\xi_\alpha=\xi_i} \tag{2.5}$$

If $\xi_\alpha \neq \xi_i$, then the trivial solution $u_{i,\alpha} \equiv 0$ solves Eq. (2.5). So abusing notation by writing u_i to be the solution of Eq. (2.5) with $\xi_\alpha = \xi_i$, we obtain the solution of Eq. (1.1)

$$E(x,y,t) = \sum_{i=1}^{\infty} u_i(x,t) m_i(y)\xi_i \tag{2.6}$$

Note that this same u_i will solve the PDE obtained from taking the inner product with $m_i(y)$ of Eq. (2.2), assuming ϵ constant. Further, if $\epsilon(x,y)$ is not constant, the complications in the spectral analysis arise only in the $\mu\epsilon(x,y)\frac{\partial^2}{\partial t^2}$ term, and does not invalidate the essence of the above calculations.

2.2 Numerical Method for Simulations

To solve Eq. (2.2), we introduce the two variables

$$\varphi_i(x,y,t) = \int_0^t \frac{\partial E_i}{\partial x}(x,y,s)ds + \int_0^x \mu\epsilon(\eta,y)\frac{\partial E_i}{\partial t}(\eta,y,0)d\eta \tag{2.7}$$

$$\psi_i(x,y,t) = \int_0^t \frac{\partial E_i}{\partial y}(x,y,s)ds + \int_0^y \mu J_i(x,\nu,0)d\nu \tag{2.8}$$

Moreover, we let $\tilde{E}_i = \frac{1}{c}E_i$. Then Eq. (2.2) becomes a symmetric (and strictly) hyperbolic system

$$\mathbf{u}_t = A\mathbf{u}_x + B\mathbf{u}_y + F \tag{2.9}$$

where $c = \frac{1}{\sqrt{\mu\epsilon}}$ is the speed of the electromagnetic wave through the medium, and

$$\mathbf{u} = \begin{pmatrix} \phi_i \\ \psi_i \\ \tilde{E}_i \end{pmatrix}, \quad A = \begin{pmatrix} 0 & 0 & c \\ 0 & 0 & 0 \\ c & 0 & 0 \end{pmatrix}, \quad B = \begin{pmatrix} 0 & 0 & 0 \\ 0 & 0 & c \\ 0 & c & 0 \end{pmatrix}, \quad F = \begin{pmatrix} 0 \\ 0 \\ -\mu c J_i \end{pmatrix}$$

For the initial conditions, we take

$$E(x, y, 0) = 0 = \frac{\partial E}{\partial t}(x, y, 0) \tag{2.10}$$

These imply that the initial conditions for the system (2.9) are

$$\phi_i(x, y, 0) = \psi_i(x, y, 0) = E_i(x, y, 0) = 0 \tag{2.11}$$

To solve for E_i numerically, the following Lax-Wendroff finite difference scheme was used

$$\begin{aligned} v^{n+1} &= v^n + k(D_0^x + D_0^y)v^n + \\ &\quad \frac{k^2}{2}\big(AD_0^x(AD_0^x + BD_0^y)v^n + BD_0^y(AD_0^x + BD_0^y)v^n\big) \end{aligned} \tag{2.12}$$

where k is the time step and D_0^x, D_0^y are the difference operators in the x and y directions, respectively, which depend on the spatial step h. It can be shown that the scheme (2.12) is consistent and dissipative for $\lambda := \frac{k}{h} < \frac{1}{2\sqrt{3}\max\{\rho(A),\rho(B)\}}$, and hence stable for A, B strictly hyperbolic [5]. We also used a positive width for the current density J at $x = 0$.

$$J(x, y, t) = \sum_{i=1}^{\infty} \mathbf{1}_{[0,\delta]}(x) V_A(t) m_i(y) \xi_i \tag{2.13}$$

Alternatively, one can also implement any stable finite difference scheme directly to Eq. (2.2), or involve the computation of the coupled magnetic field through the finite difference time domain (FDTD) method.

3 Convergence and Error Analysis

In this section, we attempt to quantify the convergence properties of the *Galerkin approximations*

$$E^{N,K} := \sum_{\alpha \in \mathcal{J}_{N,K}} E_\alpha \xi_\alpha \tag{3.1}$$

where $\mathcal{J}_{N,K} = \{\alpha \in \mathcal{J} : |\alpha| \leq K, \alpha_n = 0 \text{ for } n > N\}$. It is imperative to consider an appropriate space in which to conduct the convergence analysis. For this, we propose to use a weighted Wiener Chaos space

$$\mathcal{R}L_2(\mathbb{F}; V) = \big\{ f \ : \ \sum_{\alpha} (r_\alpha \|f_\alpha\|_V)^2 < \infty \big\} \tag{3.2}$$

Here, $\{r_\alpha, \alpha \in \mathcal{J}\}$ is a given sequence, V is a normed linear space and $f_\alpha = \mathbb{E}(f\xi_\alpha)$. In our case, we may take for instance $V = L_{2,p}([0,X] \times [0,Y] \times [0,T])$ the space of periodic L_2 functions with periodic 1st derivatives, and we let $\{v_k\}$ be an orthonormal basis of V. Later, we will make an expedient choice for v_k.

Suppose $\frac{\partial J}{\partial t} \in \mathcal{R}L_2(\mathbb{F}; V)$ for some $\{r_\alpha\}$, and suppose the wave equation (1.1) admits a solution $E \in \mathcal{R}L_2(\mathbb{F}; V)$. Direct computation gives the error estimate

$$\|E - E^{N,K}\|^2_{\mathcal{R}L_2(\mathbb{F};V)} = \sum_{\alpha \notin \mathcal{J}_{N,K}} \sum_{k=1}^{\infty} r_i^2 |\langle E_\alpha, v_k \rangle|^2 \tag{3.3}$$

Comparing Eq. (3.3) with

$$\big\| \frac{\partial J}{\partial t} \big\|^2_{\mathcal{R}L_2(\mathbb{F};V)} = \sum_{\alpha \in \mathcal{J}} \sum_{k=1}^{\infty} r_\alpha^2 |\langle \frac{\partial J_\alpha}{\partial t}, v_k \rangle|^2 < \infty, \tag{3.4}$$

we see that the error vanishes as $N, K \to \infty$, if there is a term-by-term upper bound of the form $|\langle E_\alpha, v_k \rangle| \leq C |\langle \frac{\partial J_\alpha}{\partial t}, v_k \rangle|$, where C is a constant independent of α, k. To this end, we choose v_k to be the eigenfunctions of the operator $\triangle - \mu\epsilon \frac{\partial^2}{\partial t^2}$. For example, if ϵ is constant, we can take $\{v_k\}$ to be the tensor product of cosine bases. Then with the periodic boundary conditions, we obtain

$$\begin{aligned} \langle E_\alpha, \lambda_k v_k \rangle &= \langle E_\alpha, \big(\triangle - \mu\varepsilon \frac{\partial^2}{\partial t^2} \big) v_k \rangle \\ &= \langle \big(\triangle - \mu\varepsilon \frac{\partial^2}{\partial t^2} \big) E_\alpha, v_k \rangle = \langle \mu \frac{\partial J_\alpha}{\partial t}, v_k \rangle \end{aligned} \tag{3.5}$$

where λ_k are the eigenvalues of v_k. If $\eta = \inf_k |\lambda_k| > 0$, then we have $|\langle E_\alpha, v_k \rangle| \leq \frac{\mu}{\eta} |\langle \frac{\partial J_\alpha}{\partial t}, v_k \rangle|$, implying

$$\|E\|^2_{\mathcal{R}L_2(\mathbb{F};V)} \leq C_E \big\| \frac{\partial J}{\partial t} \big\|^2_{\mathcal{R}L_2(\mathbb{F};V)} < \infty \tag{3.6}$$

This bound will also exist for cases when all but finitely many eigenvalues are bounded away from zero.

These calculations in fact show that the solution lies in the same weighted space as the forcing source term, and hence the Fourier coefficients E_α decay fast enough to cause the error in Eq. (3.3) to vanish. Moreover, the rate at which the error vanishes is controlled by the rate at which the Fourier coefficients of $\frac{\partial J}{\partial t}$ vanishes.

$$\|E - E^{N,K}\|^2_{\mathcal{R}L_2(\mathbb{F};V)} \leq \sum_{\alpha\in\mathcal{J}_{N,K}} \sum_{k=1}^{\infty} r_\alpha^2 C^2 |\langle \frac{\partial J_\alpha}{\partial t}, v_k\rangle|^2 = C^2 \sum_{\alpha\in\mathcal{J}_{N,K}} r_i^2 \|\frac{\partial J_\alpha}{\partial t}\|_V \tag{3.7}$$

We return to the model in section (2.2), with the current source term as in Eq. (2.13). We have

$$J_i(x,y,t) = \mathbf{1}_{[0,\delta)}(x) V_A(t) m_i(y), \qquad J_\alpha \equiv 0 \text{ if } |\alpha| \neq 1$$

We choose the basis functions of V to be $v_k = v_{(j,i,l)} = n_j(x)m_i(y)s_l(t)$, where n_j, m_i, s_l are cosine bases similarly defined as in (1.9), but with appropriate indices j, i, l and boundary values X, Y, T.

$$\begin{aligned}
\|\frac{\partial J_i}{\partial t}\|_V &= \sum_{j,k,l} \iint \mathbf{1}_{[0,\delta)}(x) V_A'(t) n_j(x) s_l(t) dx dt \int m_i(y) m_k(y) dy \\
&= \sum_{j,l} \iint \mathbf{1}_{[0,\delta)}(x) V_A'(t) n_j(x) s_l(t) dx dt \\
&= \|\mathbf{1}_{[0,\delta)}\|_{L_2([0,X])} \|V_A'(t)\|_{L_2([0,T])} \\
&= \delta \|V_A'(t)\|_{L_2([0,T])} =: \delta B_J
\end{aligned} \tag{3.8}$$

where B_J is independent of i. Hence

$$\|\frac{\partial J}{\partial t}\|^2_{\mathcal{R}L_2(\mathbb{F};V)} = \delta B_J \sum_i r_i^2$$

and we see that $\frac{\partial J}{\partial t} \in \mathcal{R}L_2(\mathbb{F};V)$ for any sequence $\{r_i\}$ for which $\sum_i r_i^2$ converges. For example, we can take $r_i = \frac{1}{i}$. Combining this result with Eq. (3.7), we now have a concrete bound on the error

$$\|E - E^N\|^2_{\mathcal{R}L_2(\mathbb{F};V)} \leq (\delta B_J C)^2 \sum_{i=N+1}^{\infty} r_i^2 \tag{3.9}$$

We have yet to properly treat the case when ϵ is not constant. If we consider the basis $\{v_{(j,i,l)}\}$ defined above Eq. (3.8), then

$$\begin{aligned}
\big(\triangle - \mu\epsilon(x,y)\frac{\partial^2}{\partial t^2}\big) v_{(j,i,l)} &= (\kappa_j^X + \kappa_i^Y - \mu\epsilon(x,y)\kappa_l^T) v_{(j,i,l)} \\
&= \lambda_{(j,i,l)}(x,y) v_{(j,i,l)}
\end{aligned} \tag{3.10}$$

where $\kappa_j^X = -\big(\frac{(j-1)\pi}{X}\big)^2$, and similarly for κ_i^Y and κ_l^T. Eq. (3.5) still holds, and consequently, so does the bound in Eq. (3.6) provided there exists

$$\eta := \inf_{\substack{(j,i,l)\\x,y}} |\lambda_{(j,i,l)}(x,y)| > 0 \tag{3.11}$$

for all but finitely many (j,i,l). We note that for bi-valued non-zero $\epsilon(x,y)$, η in Eq. (3.11) will always exist.

3.1 Numerical Results

We ran the scheme using a square PC lattice with side length 10 times the lattice constant, with 24 grid points per lattice constant. The values of the model parameters are: lattice constant $a = 1.27$cm, permeability $\mu = 4\times10^{-7}\pi$ (that of free space), and permittivities $\epsilon_a = 9\epsilon_0$ and $\epsilon_b = \epsilon_0$, where $\epsilon_0 = 8.85419 \times 10^{-12}$ is the permittivity of free space. For the time stepping, we used $\lambda = \frac{k}{h} = \frac{\mu\epsilon_0}{4}$, and ran the simulations for 500 time steps up to time $T = 2.2063 \times 10^{-10}$.

The parameter values for the current source given in Eq. (2.13) and (1.8) are $\delta = 0.1058$cm, $\omega = 7.554 \times 10^{10}$ and $T_0 = 2.648 \times 10^{-11}$. In this case, $\delta B_J = 3.3766 \times 10^{-15}$. It turns out that the constant C_E is difficult to find. Table 1 shows the computed values of $\|E_i\|_V$ for $i = 0, 1, \ldots, 15$. The coefficient norms remain roughly constant, corroborating the hypothesis that they are bounded. This also suggests that E belongs at best to the same space as $\frac{\partial J}{\partial t}$, and not to a 'better' space with smaller weights.

i	$\|E_i\|_V$ $(\times10^{-59})$	i	$\|E_i\|_V$ $(\times10^{-59})$
0	1.0044	8	1.6292
1	1.8857	9	1.9292
2	1.4958	10	1.9426
3	1.8209	11	2.0082
4	1.5290	12	1.8519
5	1.8596	13	2.1488
6	1.6168	14	1.9939
7	1.8700	15	2.3042

Table 1: Table of $\|E_i\|_V$ values for $i = 0, 1, \ldots, 15$.

4 Change of Wiener Chaos Basis

We cast the relationship between the two approaches discussed in [1] in a more general framework. For this section, we consider a simple stochastic wave equation

$$\frac{\partial^2 u}{\partial t^2}(x, y, t) = \triangle u(x, y, t) + f(x, y, t)\dot{W}(y) \tag{4.1}$$

The "brute force" approach approximates f and $\dot{W}$ using step functions

$$f(x, y, t) \approx \sum_{p=1}^{P} f_p(x, y, t) = \sum_{p=1}^{P} f(x, y_p^*, t)\mathbf{1}_{I_p}(y) \tag{4.2}$$

$$\dot{W}(y) \approx \sum_{p=1}^{P} \dot{W}_p(y) = \sum_{p=1}^{P} \dot{W}(y_p*)\mathbf{1}_{I_p}(y) \tag{4.3}$$

where $0 = y_0 < y_1 < \cdots < y_P = Y$ forms a partition of $[0, Y]$, and $y_p^* \in I_p = (y_p, y_{p-1}]$; whereafter the solutions $\{v_p(x, y, t)\}_{p=1}^P$ to the PDEs

$$\frac{\partial^2 v_p}{\partial t^2}(x, y, t) = \triangle v_p(x, y, t) + f_p(x, y, t)\dot{W}_p(y) \tag{4.4}$$

are combined to give an approximation to the solution of Eq. (4.1)

$$u(x, y, t) \approx \sum_{p=1}^{P} v_p(x, y, t) \tag{4.5}$$

We note that $\widetilde{\dot{W}}(y) := \sum_p \dot{W}_p(y)$ lives in the P-dimensional subspace $\mathcal{I}_P := \{g(y) : g(y) = \sum_{p=1}^P g_p \mathbf{1}_{I_p}(y)\}$. What the approximation in (4.3) actually does is to approximate the Wiener Chaos $\dot{W}(y)$ on $L_2([0, Y])$ by a Wiener Chaos $\widetilde{\dot{W}}(y)$ on $\mathcal{I}_P$. Hence, taking $n_p(y) = \frac{1}{\sqrt{|I_p|}}\mathbf{1}_{I_p}(y)$, for $p = 1, \ldots, P$ to be an orthonormal basis of $\mathcal{I}_P$, we have the following expansion

$$\widetilde{\dot{W}}(y) = \sum_{p=1}^{P} \eta_p n_p(y), \tag{4.6}$$

where $\eta_p = \int_0^Y n_p(y)dW(y)$ are i.i.d $\mathcal{N}(0, 1)$ random variables. We shall call $\{n_p(y)\}$ the indicator basis.

We temporarily divert our attention to the alternative method presented in [1], based on the Wiener Chaos expansion (1.11) against the cosine basis (1.9), and which was studied in the preceding parts of this paper. In order to compare its performance with the step function approximation, we seek to project $\dot{W}$ onto the space $\mathcal{I}_P$.

It can be checked that $m_{i,p}(y) := \sum_{p=1}^P m_i(y_p^*)\mathbf{1}_{I_p}(y)$, $i = 1, 2, \ldots$, are linearly independent, so by the Gram-Schmidt process, we can find an orthonormal basis $\{\tilde{m}_i\}_{i=1}^P$ on $\mathcal{I}_P$ derived from $\{m_{i,p}\}_{i=1}^P$. Letting $\tilde{\xi}_i = \int_0^Y \tilde{m}_i(y)dW(y)$, we obtain an alternative expansion

$$\widetilde{\dot{W}}(y) = \sum_{i=1}^{P} \tilde{\xi}_i \tilde{m}_i(y) \approx \sum_{i=1}^{P} \xi_i m_i(y) \tag{4.7}$$

For large P, $\{m_{i,p}(y)\}$ are very close to orthonormal, in which case using the original cosine functions $m_i(y)$ in place of $\tilde{m}_i(y)$ will also provide a good approximation. Hence, $\widetilde{\dot{W}}$ approximates $\dot{W}$ in a $\mathcal{R}L_2(\mathbb{F})$ weighted space. We shall call $\{\tilde{m}_i(y)\}$ the orthonormalized cosine basis and $\{m_i(y)\}$ the continuous cosine basis.

The random variables $\tilde{\xi}_i$ are related to η_p by a simple change of variables

calculation.

$$\begin{aligned}\tilde{\xi}_i &= \int_0^Y \tilde{m}_i(y)\widetilde{\dot{W}}(y) \\ &= \int_0^Y \tilde{m}_i(y)\left(\sum_{p=1}^P \eta_p n_p(y)\right) dy = \sum_{p=1}^P \eta_p \langle \tilde{m}_i, n_p\rangle \end{aligned} \tag{4.8}$$

The last equation gives a feasible way to change the basis of expansion of the Wiener Chaos. As noted by Badieirostami et al, this can be highly convenient and efficient in applications, since different basis are optimal for different forms of random noise in the PDE. Eq. (4.8) is a basic fact of finite dimensional linear algebra, and also holds for infinite dimensional Wiener Chaos spaces. Thus in more general linear SPDE cases, we can apply the same argument to approximate and change the basis of the Wiener Chaos space.

4.1 Simulations

We perform numerical simulations to illustrated the efficacy of the change of basis approach. Two parallel simulations are conducted, one for each expansion basis. In the indicator basis, the skeleton equations are obtained by multiplying both sides of Eq. (1.1) by η_p, then taking expectation. Likewise, we do the same for the orthonormalized cosine basis. Hence, we solve the set of equations

$$\triangle E_p(x,y,t) - \mu\epsilon(x,y)\frac{\partial^2 E_p}{\partial t^2} = \mu \mathbf{1}_{[0,\delta)} V_A'(t) n_i(y) \tag{4.9}$$

$$\triangle E_i(x,y,t) - \mu\epsilon(x,y)\frac{\partial^2 E_i}{\partial t^2} = \mu \mathbf{1}_{[0,\delta)} V_A'(t) \tilde{m}_i(y) \tag{4.10}$$

for $p, i = 1, \ldots, P$. Assuming P large enough, we replace $\tilde{m}_i(y)$ in Eq. (4.10) with the continuous cosine basis functions $m_i(y)$. Figure 1 illustrates the increasing degree of agreement between the truncated cosine expansion and the Wiener Chaos, as the number of coefficients retained increases.

In the simulations, the numerical setup for the simulations were the same as in §3.1, except that the PDE was evolved up to time $T = 4.4128 \times 10^{-10}$. The same Wiener Chaos approximations as in Fig. 1 was used. Figures 2 and 3 show the solution of Eq. (1.1) at time T obtained from truncating the continuous cosine basis expansion and the indicator basis expansion, respectively, to $10, 20, \ldots, 50$ coefficients. It is clear from the graphs that the cosine expansion gives a better result. This is reflected in Figure 4(b). At 50 coefficients, the cosine expansion gives a mere 2.2% error, compared with 27.1% error incurred from truncating the indicator function expansion to the same number of coefficients.

References

[1] M. Badieirostami, A. Adibi, H. Zhou, S. Chow. *Efficient modeling of spatially incoherent sources based on Wiener chaos expansion method for the*

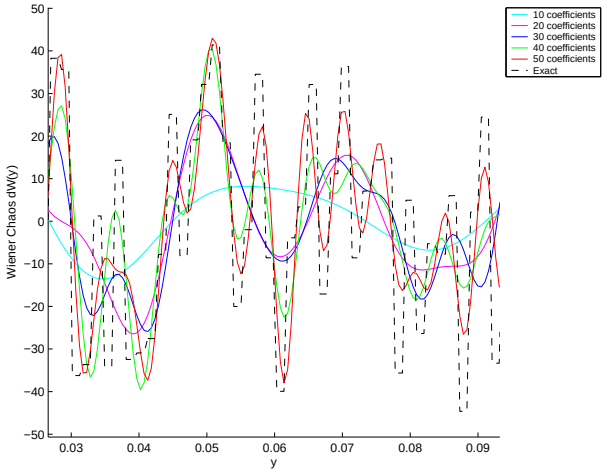

Figure 1: Approximation of the Wiener Chaos on $\mathcal{I}_P$ using the expansion in the continuous cosine basis functions $m_i(y)$, for one realization of the Wiener Chaos. The expansions truncated at $10, \ldots, 50$ coefficients (colored plots) can be compared to the exact value of the Wiener Chaos (black plot).

analysis of photonic crystal spectrometers, Proc. of SPIE, Vol. 6480, 648018 (2007).

[2] S.V. Lototsky, B.L. Rozovskii. *Wiener Chaos Solutions of Linear Stochastic Differential Equations*

[3] J.D. Kraus *Electromagnetics* (4e McGraw-Hill 1991)

[4] K. Sakoda *Optical Properties of Photonic Crystals* (Springer, Berlin Heidelberg 2001)

[5] B. Gustafsson, H. Kriess, J. Oliger. *Time Dependent Problems and Difference Methods* (John Wiley 1995)

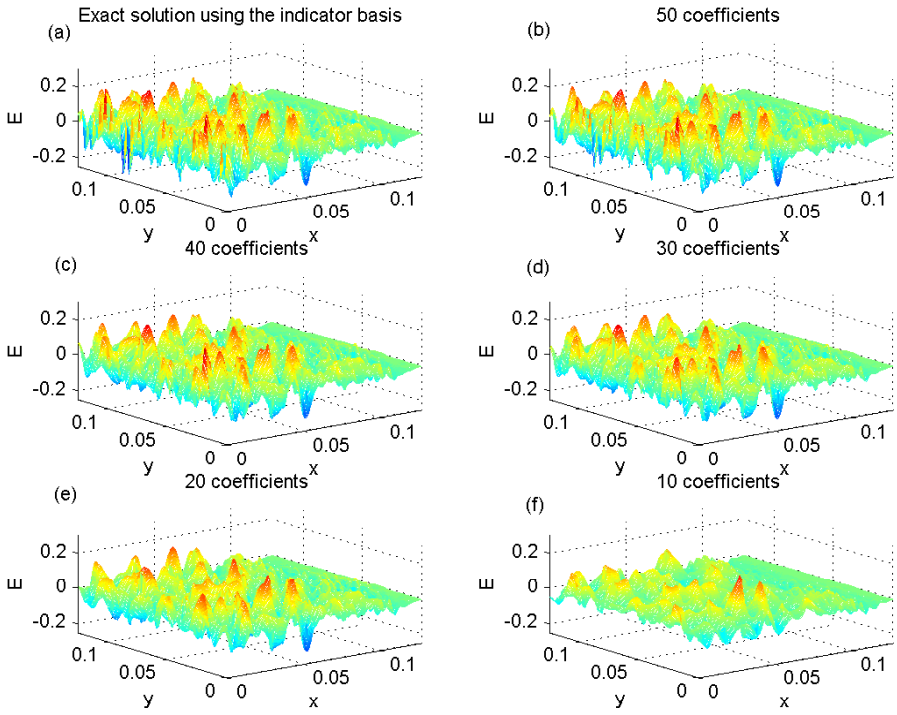

Figure 2: Approximate solutions of the wave equation using the continuous cosine basis functions. The expansion was truncated at $10, \ldots, 50$ coefficients in plots (b)-(f). Plot (a) shows the solution obtained from the complete indicator basis expansion of $\widetilde{\dot{W}}$.

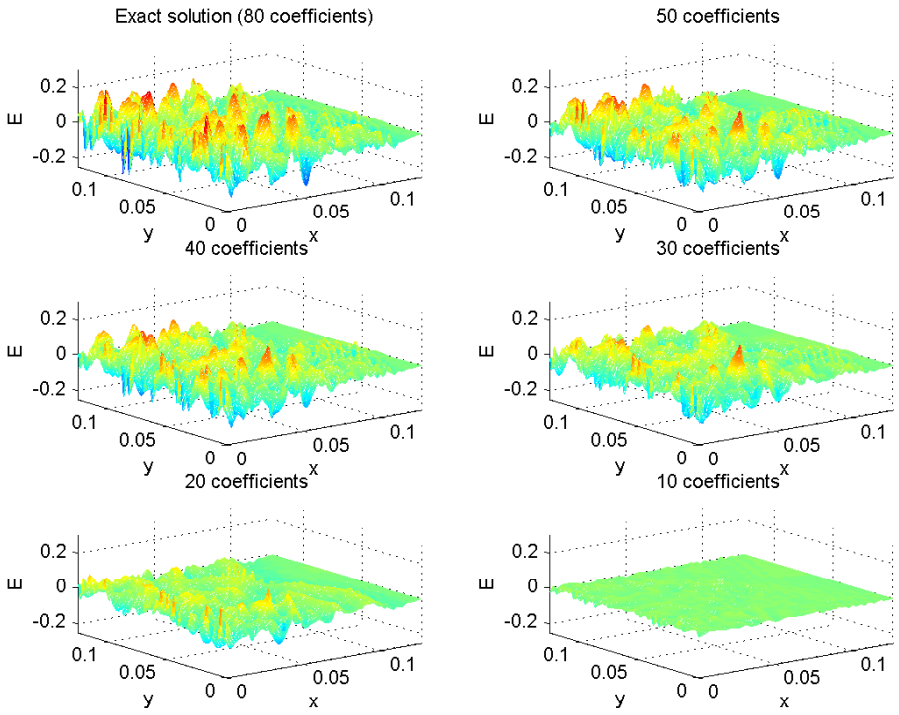

Figure 3: Approximate solutions of the wave equation using the indicator basis functions. Plot (a) shows the solution obtained from the complete indicator basis expansion of $\widetilde{W}$. The expansion was truncated at $10, \ldots, 50$ coefficients in plots (b)-(f).

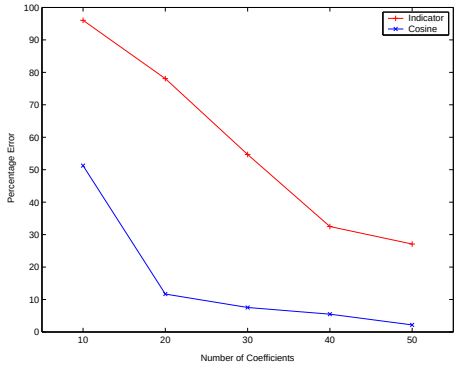

Figure 4: Percentage error incurred by truncating the Wiener Chaos expansion. The cosine basis expansion shows markedly better results than the indicator basis expansion, even at fewer number of coefficients retained in the expansion.